Nanoscale

rsc.li/nanoscale

ROYAL SOCIETY
OF CHEMISTRY
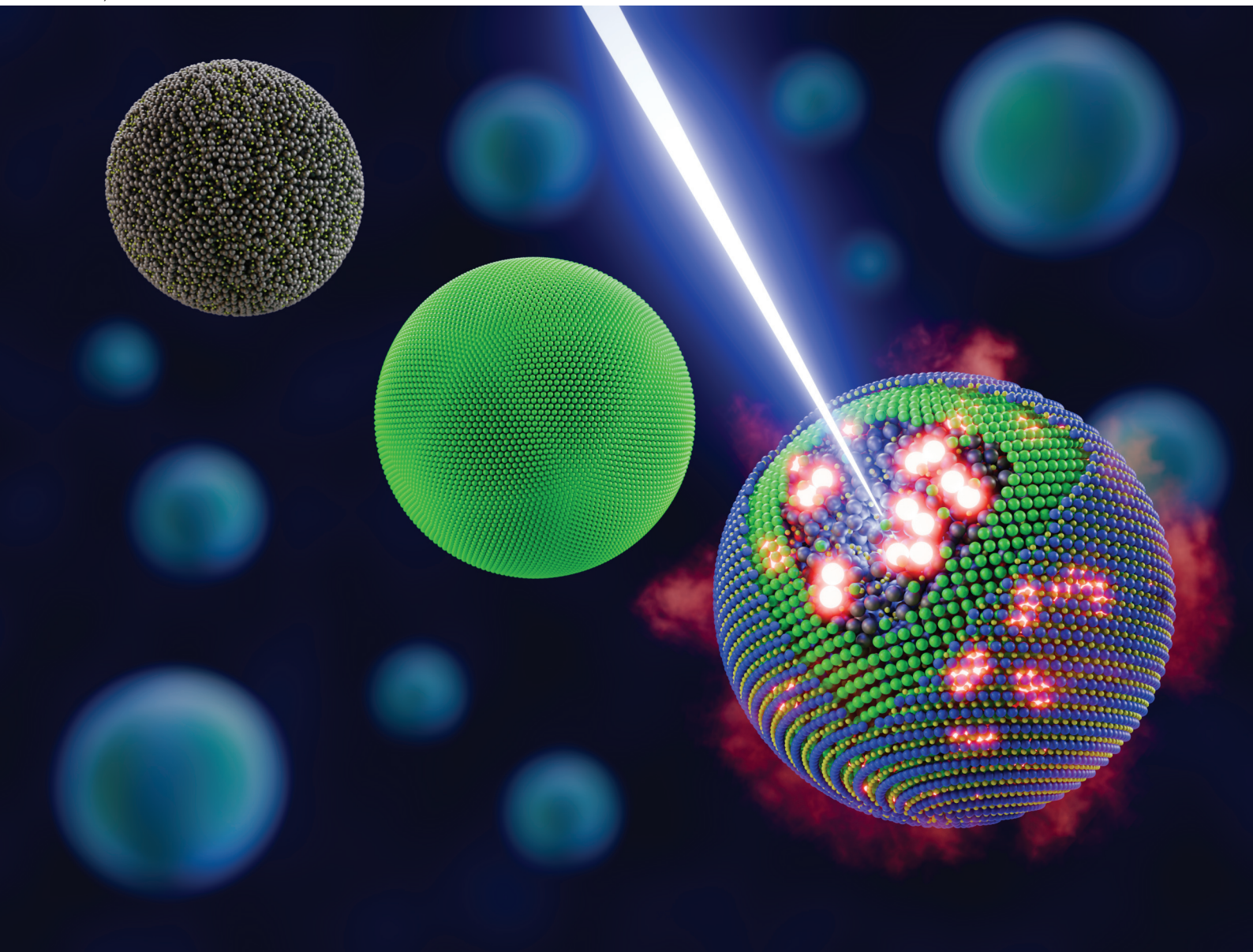
PAPER
Victor Vega-Mayoral, Beatriz H. Juárez *et al.*
Exploring many-body phenomena: biexciton generation and
auger recombination in Ag₂S-based nanocrystals

NCNST

View Article Online
View Journal | View Issue

Exploring many-body phenomena: biexciton generation and auger recombination in Ag₂S-based nanocrystals†

Victor Vega-Mayoral, [ID] *[a,b] Saül Garcia-Orrit,[a] Peijiang Wang, [ID][c]
Rafael Morales-Márquez, [ID][c] Emma Martín Rodríguez, [ID][d,e,f] Beatriz H. Juárez [ID] *[c]
and Juan Cabanillas-Gonzalez [ID][a,b]

The optoelectronic properties of Ag₂S nanocrystals with different surface passivation treatments have been investigated using femtosecond transient absorption spectroscopy. Plain Ag₂S nanocrystals and improved surface-passivated nanostructures were studied under different pump fluences and photon energies. Surface passivation significantly sharpens excitonic resonances, reducing defect-assisted recombination. Transient absorption spectroscopy reveals that the excited state dynamics are dominated by trapping and exciton recombination at low exciton densities, while fluence dependence studies reveal significant contributions from biexcitons and Auger recombination in all samples at high exciton densities. Notably, surface-passivated nanostructures exhibit faster multi-exciton recombination dynamics, high-lighting the impact of effective surface passivation.

*[a]IMDEA Nanoscience, Faraday 9, Campus de Cantoblanco, 28049 Madrid, Spain.
E-mail: victor.vega@imdea.org*
*[b]Unidad de Nanomateriales Avanzados, IMDEA-Nanociencia, Unidad Asociada al
CSIC por el ICMM. C/Faraday 9, 28049 Madrid, Spain*
*[c]Materials Science Institute of Madrid, ICMM, Spanish Research Council, CSIC, C/
Sor Juana Inés de la Cruz, 3, 28049 Madrid, Spain. E-mail: bh.juarez@csic.es*
*[d]Departamento de Física Aplicada, Facultad de Ciencias, Universidad Autónoma de
Madrid, C/Francisco Tomás y Valiente 7, Madrid, Spain*
*[e]Instituto Ramón y Cajal de Investigación Sanitaria (IRYCIS), Ctra. Colmenar Viejo,
km. 9100, 28034 Madrid, Spain*
*[f]Institute for Advanced Research in Chemistry (IAdChem), Campus de Cantoblanco,
28049 Madrid, Spain*
†Electronic supplementary information (ESI) available. See DOI: https://doi.org/
10.1039/d5nr00511f

Introduction

The development of efficient and tunable luminophores emitting in the near-infrared (NIR-II) region is rapidly advancing, driven by applications in diverse fields such as telecommunications, photovoltaics, optoelectronics or nanomedicine.[1–7] Among these luminophores, Ag₂S nanocrystals (NCs) stand as front-runners for some of these applications. First, due to their low toxicity and notable photoluminescence quantum yield (PLQY) values with emission in the NIR-II window, Ag₂S NCs have been widely exploited as fluorescent-, photothermal-, and/or nanothermometry probes in biological environments.[8,9] Furthermore, due to its electronic band gap (~1.1 eV), Ag₂S has been subject to study for solar cell and photodetection applications, both in the form of thin films and as nanocrystals.[10,11]

In general, many-body processes play an important role in the optoelectronic properties of a material and have significant implications for developing next-generation devices.[12,13] In this respect, Ag₂S nanocrystals hold great promise, since they integrate unique optical and electronic properties, such as multi-exciton generation (MEG), a pivotal feature for advancing in efficiency and functionality. Ag₂S NCs are capable of carrier multiplication *via* MEG, where photon energies above the band gap can lead to the generation of multiple excitons from a single absorbed photon, which enhances the photon conversion efficiency.[14,15] The presence of MEG is not only promising for boosting the photovoltaic efficiency, but also offers insights into exciton dynamics and the interaction of photoexcited carriers within strongly confined nanostructures.[12,13] Colloidal Ag₂S NCs with sizes beyond the quantum confinement regime (*i.e.*, particle sizes significantly larger than the exciton Bohr radius of ~2 nm),[16] typically above ~4–6 nm, can also benefit from the MEG phenomenon as the density of excited states increases. Nevertheless, the behaviour of photoexcited states at low and high densities might differ significantly. Above the threshold density of carriers, many-body phenomena dominate relaxation processes and hence the applicability of a given material might get compromised or boosted for a certain application. Colloidal Ag₂S NCs have been previously studied with transient absorption spectroscopy (TAS).[14,17,18] Furthermore, TAS has been employed to follow the exciton dynamics in cation exchange CdS–Ag₂S rods.[19]

In a recent work, we highlighted the outstanding PLQY improvement of Ag_2S NCs covered by a shell that incorporates Se and Zn synthesized by hot-injection.[20] The emission improvement was explained as the result of the effect of two passivation layers: an inner one composed of $Ag_2(S,Se)$ formed upon treatment with a selenium precursor and an outer one, composed of ZnS, formed after further treatment with a zinc precursor and subsequent Zn diffusion.[20] In this work, TAS measurements have been conducted to provide insights into the electronic states and the dynamics of charge carriers of plain and surface-passivated Ag_2S NCs to characterize their multiexciton interactions and associated decay pathways. It is found that while thermalization, trapping, and exciton recombination govern relaxation at low fluences, studies at higher fluences reveal that the photophysics is dominated by two many-body processes: biexcitons and Auger recombination.

Furthermore, by comparing the effects of surface passivation across different NCs, we demonstrate how the reduction of surface defects directly impacts on the radiative and non-radiative relaxation channels. Along with the improvement in the PLQY resulting from a decrease in defect-assisted recombination and the sharpening of excitonic resonances,[21] surface passivation also lowers the exciton density threshold required for biexciton generation and Auger recombination.[22,23] The enhancement of many-body phenomena together with the enhanced PLQY supports an effective passivation of surface defects.

Results and discussion

Ag_2S NCs were synthesised following a previously reported method, as schematized in Fig. 1a.[20] After the synthesis of plain Ag_2S core NCs (referred to as Ag_2S C hereafter), the treatment with a trioctylphosphine selenide (Se@TOP) solution forms a core/shell NC $Ag_2S/Ag_2(S,Se)$ structure (CS). As indicated in the drawing, the CS nanostructures were subsequently exposed to zinc oleate solution, facilitating the growth of a zinc chalcogenide layer, generating a core/shell/shell structure formed by $Ag_2S/Ag_2(S,Se)/ZnS$ (CSS).[20] Representative High-Resolution Transmission Electron Microscopy (HRTEM) images of Ag_2S C, CS and CSS samples can be seen in Fig. 1b. Further TEM images can be found in section S1 and Fig. S1 in the ESI.† The average size of CS NCs is approximately 8.0 ± 0.6 nm. A similar size distribution was observed for the pure Ag_2S NC cores. In the Zn-treated samples, a slight increase in size distribution by about 1.0 nm was observed. Zn treatment leads to a slight modification of the initial morphology, yielding NCs of larger polyhedral geometry as a result of the Zn diffusion into the $Ag_2S/Ag_2(S,Se)$ lattice. In our previous study, ion bombardment combined with XPS characterization revealed a gradient in chemical composition, transitioning from a ZnS-rich outer shell surface to Ag_2S-rich regions closer to the inner core.[20] Synthesis and spectroscopic details can be found in ref. 20 and in the ESI.†

The extinction spectra of Ag_2S C, CS and CSS NCs are shown in Fig. 1c. All extinction spectra exhibit featureless pro-
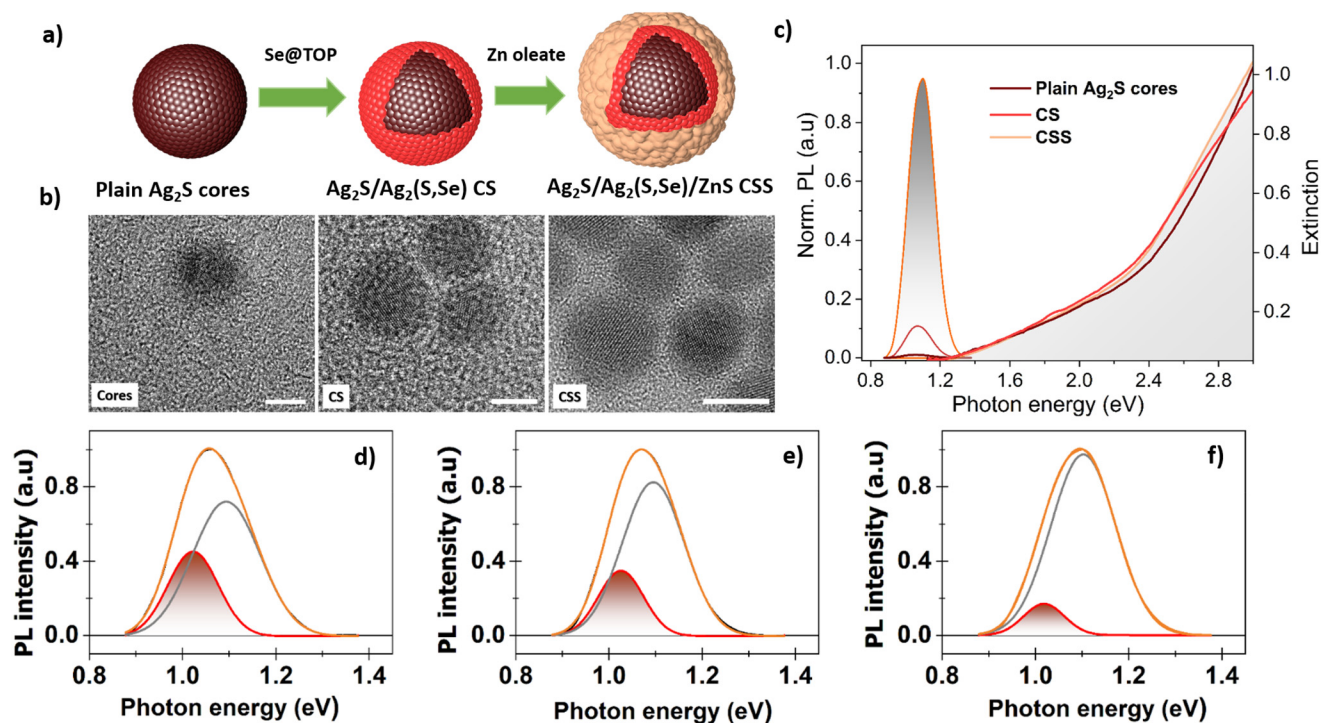
Fig. 1 (a) Sketch of the Ag_2S C NCs passivated upon two treatments: first with a Se precursor solution and second with a Zn precursor solution. (b) Representative HRTEM images of the Ag_2S C, CS and CSS samples. Scale bars correspond to 5 nm. (c) Extinction and normalized PL intensities of Ag_2S C (wine), CS (red) and CSS (orange). (d–f) PL intensity spectra of the (d) Ag_2S C, (e) CS and (f) CSS NCs fitted to two Gaussian components (see the ESI† for details). The component marked in red (related to surface defects) decreases as the NCs are better passivated.

files with strong absorption in the visible region and a long tail spanning across the visible region down to the NIR region. No excitonic resonances are observed, likely due to a combined effect of the low exciton binding energy (0.09 eV, a value obtained by applying effective mass approximation methods[16]) and the relatively big particle size (∼9 nm) compared to the exciton Bohr radius (2 nm), leading to the absence of confinement effects.[16,21] Absorption spectra of Ag_2S C ranging from ∼7 to 9 nm can be found in section S2 and Fig. S2, ESI.† The lack of excitonic resonance in the extinction spectra has also been assigned to the presence of intra gap defect states.[24] Defect states are distributed along a range of energies below the conduction band (or above the valence band), blurring the excitonic resonances. The photoluminescence (PL) spectra of the three types of NCs (Fig. 1c) were examined and compared to assess the impact of the passivation layers. Starting with Ag_2S C, the PL adopts the shape of a broad emission band centered at around ∼1.1 eV, characteristic of excitonic recombination. Previous work relates the broadband emission to the effect of electron–phonon coupling and defects at room temperature.[25] The introduction of the first shell upon Se@TOP treatment (CS sample) causes a noticeable enhancement of the PL intensity, indicating a reduction in surface defects and non-radiative recombination channels. This trend is further amplified in the CSS structure, where the formation of the additional zinc chalcogenide layer results in an even stronger PL emission, suggesting that surface passivation is more efficient in reducing non-radiative losses. The PL spectrum of the CSS sample shows a sharper and more intense peak. The PL spectra of the three NCs diverge from a single Gaussian shape as they show two distinct Gaussian contributions centered at 1.02 and 1.09 eV, respectively (Fig. 1d–f). The emission at 1.02 eV is assigned to excitons trapped at defects in surface states while the emission at 1.09 originates from free exciton recombination.[26] Free exciton recombination increases its relative weight by more than four-fold as plain Ag_2S C are passivated, forming subsequently CS and CSS NCs (Fig. 1d–f). In Fig. S3 (section S3, ESI†), the central positions of peaks assigned to contributions to the PL response from free excitons and trapped excitons, along with the ratio of the intensities of the two peaks are shown. The weight increase of free exciton recombination is accompanied by a mild 9 meV blueshift in the free exciton resonance, which is related to the stoichiometric change originated from the $Ag_2S/Ag_2(S,Se)$ layer and the concomitant slight change in the electronic band gap.[27] The larger contribution of free excitons to the PL signal points towards an efficient surface passivation and explains the increase of PLQY values from less than 1% (for plain Ag_2S C) to *ca.* 10% in CSS NCs.[20] It is worth mentioning that the relatively large Ag_2S NCs we study in this work exhibit weak electron and hole wavefunction overlap, leading to a small transition dipole moment and limiting the radiative decay. This factor, combined with slow radiative recombination rates and trap-mediated non-radiative recombination processes commonly observed in narrow-bandgap semiconductors, inherently constrains the maximum achievable PLQY for these NCs. Despite these intrinsic limitations, our synthesis and passivation strategies have demonstrated improved performance, achieving a PLQY of ∼10%, which is a reasonable value for large NCs exhibiting weak or no quantum confinement. These values can be achieved by forming a type-I core/shell structure that reduces surface defects,[20,28–31] or by post-treatments.[32,33] Higher PLQYs can be obtained through strong quantum confinement (*i.e.*, reducing the particle size)[34,35] or ligand exchange reactions.[36] Considering an effective passivation in CSS NCs where non-radiative emission paths are only due to bulk defects, in our case, it is estimated that for Ag_2S plain cores, around 91% of non-radiative paths are due to surface defects, while around 9% is due to bulk defects (see section S4, ESI† for details).

Low pump-fluence regime

TAS measurements with 120 fs resolution were performed to explore the dynamics of photoexcited states in Ag_2S-based NCs. In TAS, a pump pulse excites the system and the resulting population of excited states is tracked in real time by monitoring the absorption changes induced by a temporally delayed and spectrally chirped probe pulse.[28] These absorption changes reflect the cross-sections of various excited states (*e.g.*, charge carriers, excitons, or polarons) and their evolving populations over time. The absorption changes (ΔA) can be described as:[29]

$$\Delta A = \sum_i (\sigma_i(\omega) \times \Delta n_i(t) + \Delta\sigma_i(\omega,t) \times n_i(t)) \quad (1)$$

where i denotes the ground state and various photoexcited states, σ is the absorption cross-section and n is the population of photoexcited states. The first term accounts for population changes, whereas the second term refers to changes over the cross-section of the associated optical transitions caused by phenomena such as the Stark effect,[30–32] the Burstein–Moss effect[33] or bandgap renormalization.[34] Our femtosecond temporal resolution, a setup combined with a delay window spanning up to 500 ps, allows us to study excitonic and photogenerated carrier dynamics, energy transfer processes,[35] many-body phenomena[36,37] or other observables such as the Stark effect,[30] bandgap renormalization[38] or the Burstein–Moss effect,[33] as previously mentioned. From now on, assuming the small signal approximation, the TAS results are represented as $-\Delta A \approx \frac{\Delta T}{T}$.

Fig. 2a displays a density plot of $\Delta T/T$ across an entire delay window for plain Ag_2S C upon pumping with 1.6 eV photons at a 0.16 mJ cm^{-2} fluence (upper plot) and the TAS spectra at selected delays (bottom plot). The TAS spectrum of Ag_2S C is dominated by a broad positive signal centered at 1.2 eV (ground state photobleach, PB) and a negative band originating from the absorption from excited states (ESA) at energies below 1.1 eV. The PB signal accounts for the spectral signature of excitons, whereas the ESA stands for the absorption of photons from photoexcited species. The absence of quantum confinement in plain Ag_2S C suggests that the ESA features
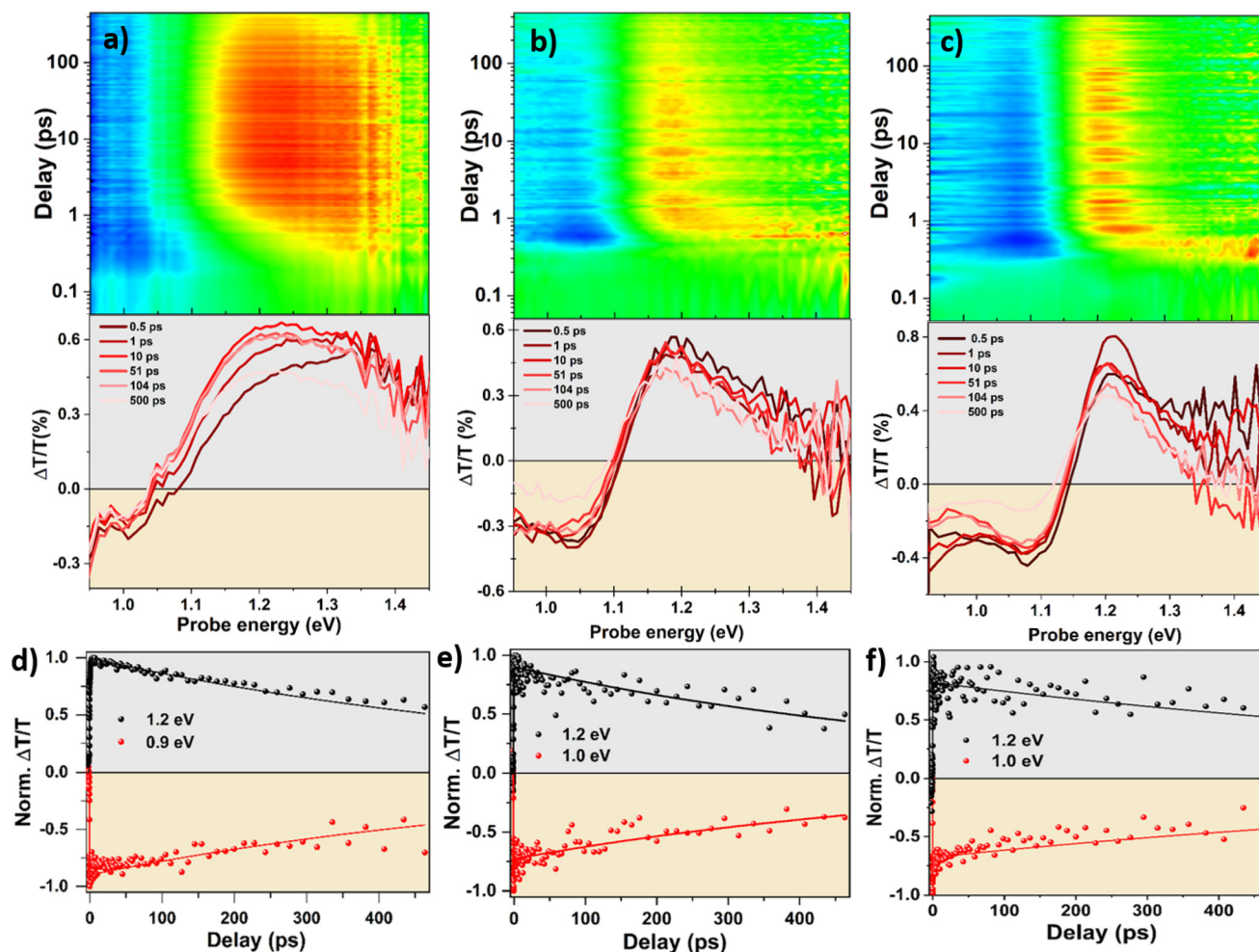
Fig. 2 Density plot of $\Delta T/T$ as a function of delay (up) and spectra at significant delays of Ag$_2$S C (a), CS (b) and CSS (c). Temporal traces at 1.2 (PB, black) and 0.9 (ESA, red) eV are shown as dots. Fits are depicted as straight lines, reproducing the Ag$_2$S C (d), Ag$_2$S CS (e) and Ag$_2$S CSS NCs (f).

may arise from intraband transitions or transitions involving defect states, such as surface states. As can be seen in Fig. 2a, the spectral evolution of Ag$_2$S C is as follows: the initial PB (already present within pump pulse duration) is centered at 1.35 eV and undergoes a redshift and broadening in the first picoseconds, shifting the maximum by 10 meV to lower energies. On the other hand, the ESA undergoes an apparent redshift during 1 ps, which in the high energy range overlaps spectrally with the PB resonance. The temporal dynamics of both resonances are biexponential and can be satisfactorily reproduced by applying global fit analysis using a system of two linear differential equations (see sections S5 and S6, ESI†):

$$\frac{dE_1}{dt} = G - k_1 \times E_1 \tag{2}$$

$$\frac{dE_2}{dt} = k_1 \times E_1 - k_2 \times E_2 \tag{3}$$

where E_1 and E_2 are the populations of the ensembles of photoexcited states and k_1 and k_2 are the rate constants. This

simple model satisfactorily reproduces the TAS signal and provides τ_{1NCs} = 840 fs and τ_{2NCs} = 944 ps as lifetimes of the photoexcited states in plain Ag$_2$S C. Longer lifetimes, spanning from hundreds of picoseconds to a nanosecond, are typically assigned to band to band or exciton recombination.[17,18] Accordingly, we assigned the shorter lifetime to the thermalization and trapping of hot excitons and the longer lifetime to exciton recombination.

A high density of defects is expected at the surface of plain Ag$_2$S C, leading to exciton trapping, which creates a distribution of different exciton binding energies, as evidenced by the broader PB contribution in the TAS spectra generated in the first picosecond.[25] Brelle et al. proposed a triphasic relaxation dynamics in their study with an intermediate lifetime of 4 ps assigned to the evolution from shallow to deep traps.[17] Since we observe a single (sub)ps process, this suggests that one type of defect dominates the photoexcited state dynamics. These defects are distributed closely below the bandgap and contribute to the broadening of the excitonic resonance (see the lower panel in Fig. 2a). Interestingly the broad PB reso-

nance in Ag_2S C narrows significantly as the first and second passivation layers are added (CS and CSS samples), as can be seen in Fig. 2b and c (lower panels). The width of the excitonic resonance in CS and CSS NCs remains roughly constant as delay evolves and undergoes a 25 meV redshift in the first picosecond after photoexcitation. When pumping with 1.6 eV photons and 0.16 mJ cm^{-2}, the excited state temporal evolution of CS and CSS NCs is biphasic, as their behavior can be reproduced with the same sequential model, obtaining lifetimes of τ_{1CS} = 240 fs and τ_{2CS} = 649 ps for the CS NCs and τ_{1CSS} = 243 fs and τ_{2CSS} = 1043 ps for the CSS NCs. Interestingly, both τ_{1CS} and τ_{1CSS} decrease significantly with respect to τ_{1C}. This acceleration aligns with the hypothesis of efficient surface defect passivation in CS and CSS NCs. When the defect density is sufficiently reduced, the corresponding process may fall below the detection threshold. Since the ~240 fs value observed for τ_1 in the passivated samples is close to our temporal resolution, a reliable comparison between τ_{1CS} and τ_{1CSS} is challenging. We tentatively assign τ_{1CS} and τ_{1CSS} to a fast thermalization process occurring, approximately, in the first 200 fs in both samples. Note that since we propose a consecutive linear model, any change in the physical interpretation of the process behind τ_1 necessarily implies a different initial photoexcited state for the process described by τ_2. Similarly, since the shells passivate surface traps and defects on the Ag_2S cores, the non-radiative recombination pathways are expected to be reduced, which explains the larger τ_{2CSS} when compared with that of plain Ag_2S C. The non-monotonic change in τ_2 for C, CS, and CSS reflects the differing nature of the initial photoexcited state in the process described by τ_2. In plain Ag_2S C, where τ_1 is attributed to exciton trapping at defects, τ_2 corresponds to the recombination of trapped excitons. In contrast, in Ag_2S CS and CSS, after a fast thermalization process described by τ_1, the process governed by τ_2 corresponds to the recombination of free excitons. The longer τ_2 observed in CSS compared to CS suggests a larger exciton diffusion distance prior to recombination, resulting from improved passivation and a lower density of recombination centers.

The passivation layers in the CS and CSS structures reduce defect density, resulting in narrower, more defined, and sharper excitonic resonances, as fewer surface-related states contribute to the ESA signal. The defect states can be due to Ag^+ and S^{2-} vacancies, which introduce long-lived states. The improved surface passivation also leads to stronger PL intensities in the CS and CSS samples, as previously evidenced in Fig. 1b. Fig. 2e and f show the temporal traces at 1.2 eV (in black) and 0.9 eV (in red) fitted according to eqn (1) and (2). It is noteworthy that the same relaxation model is able to reproduce the low pump fluence photophysics of the three samples.

High pump-fluence regime

To gain further insights into the behavior of excited states, a fluence dependence study was performed by pumping with two different photon energies, namely 1.6 eV and 3.2 eV, (0.5 eV and 2.1 eV above the band gap, respectively) to study the effect of energy excess and different photoexcited state densities. Fluences of 0.32, 0.6 and 1.29 mJ cm^{-2} were used to investigate the presence of many-body phenomena in the NCs. Note that two measurements with the same fluence but different pump photon energies correspond to different densities of photoexcited states within the NCs, owing to the different absorption coefficients at 1.6 and 3.2 eV. While the C and CSS samples exhibit high stability, CS photodegrades when irradiated at high fluences of 1.6 and 3.2 eV photon energies due to the presence of Se, an effect that is compensated when the ZnS outer layer is added. The lack of photostability in CS is likely related to the higher reactivity of Se (Se@TOP), an effect that was previously observed when focusing an electron beam in a high-resolution transmission electron microscope.[20] Due to the low photostability of CS NCs, their measurements have been excluded from our analysis in the main text and are reported in the ESI,† containing transient absorption data and a comparison with the global fit analysis output for all measurements (section S6 in the ESI†).

Fig. 3a and b summarize the results of Ag_2S C and CSS NCs upon pumping with 1.6 eV across a range of fluences from 0.16 to 1.29 mJ cm^{-2}. The PB (1.2 eV, black dots) and ESA signals (0.95 eV, red dots) scale equally following a linear fluence dependence for both Ag_2S NCs C (Fig. 3a) and CSS NCs (Fig. 3b), confirming a linear absorption regime and a linear dependence of all studied photoexcited states with pump fluence. This linearity stands as a remarkable finding, confirming that the loss of excited states by many-body effects is negligible when pumping with low energies, a result of interest for NIR imaging or luminescence nanothermometry in the NIR II window.[9] In contrast, when pumping with 3.2 eV photons (Fig. 3c and d), the PB and ESA signals of Ag_2S C and CSS NCs show different evolutions. The PB band (black dots) exhibits a sublinear deviation at high fluences, indicating saturation of the exciton generation in Ag_2S C (Fig. 3c). In parallel, the ESA band (red dots) evolves from a linear to superlinear (quadratic) increase. Similar dependence is observed in CSS (Fig. 3d), observing saturation of the PB intensity and super-linear ESA growth. The PB intensity in CSS inverses the growth tendency and decreases the highest pump fluence. The quadratic growth of the absorption feature suggests that that spectral feature is the signature of a two-body particle. This, in addition to the saturation or decrease of the excitonic signal at higher fluences, is interpreted as the appearance of biexcitons. The ESA band centered between 1.0 and 1.1 eV stands as the biexciton spectral fingerprint. Accordingly, the drop in the PB signal in CSS at the highest fluence (Fig. 3d) is the combined result of the spectral overlap between the biexciton ESA and the exciton PB (centered at 1.2 eV) and the higher growth of the former at high fluences. Time-resolved PL measurements performed previously in C, CS and CSS confirmed multi-exponential decay with intensity-average PL lifetimes of 50 ± 4, 360 ± 3, and 817 ± 4 ns, respectively.[20] These increasing values are in good agreement with the expected behavior for a better passivated NC. The different decay components are usually related to defects that can eventually constitute alternative paths for
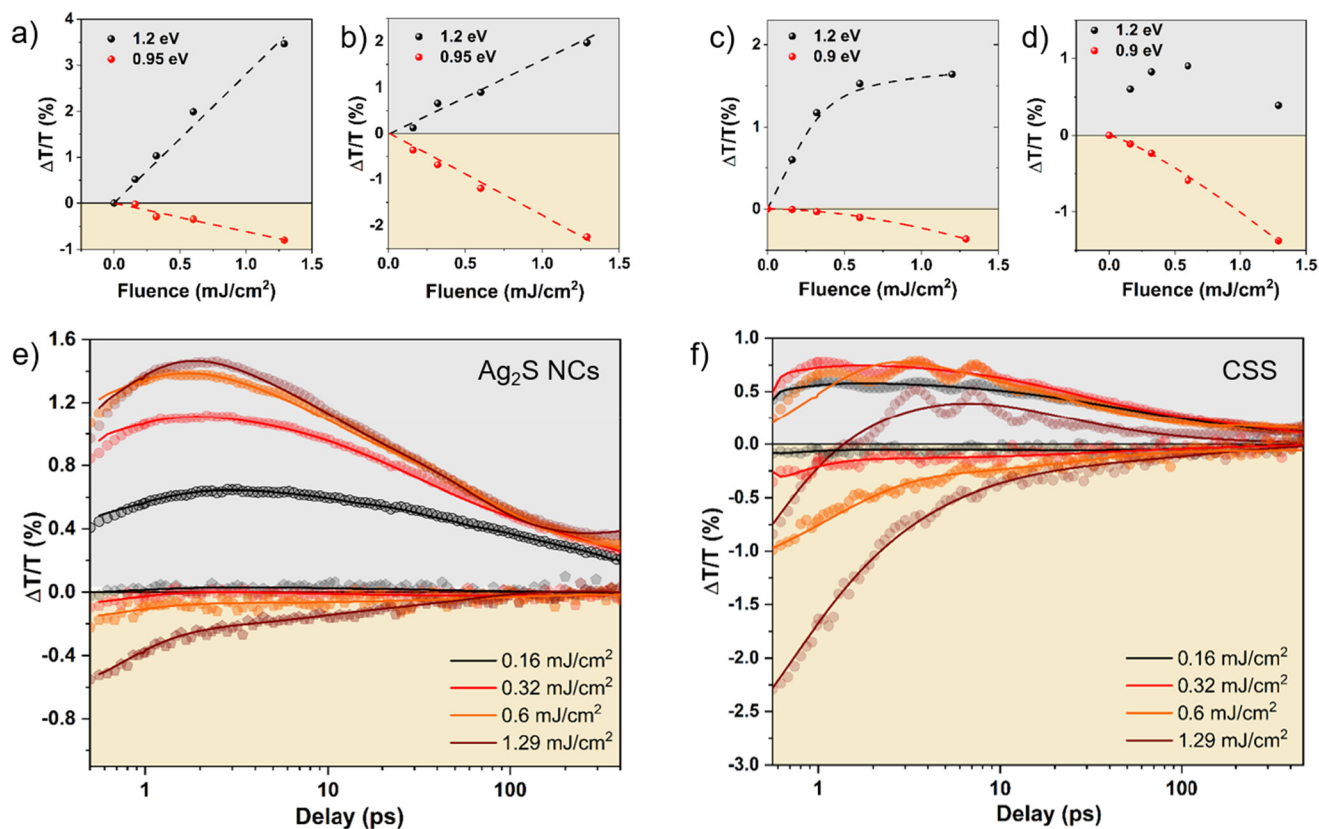
Fig. 3 $\Delta T/T$ values of Ag$_2$S NCs (a) and CSS (b) at 1 ps delay for E_{exc} = 1.6 eV. Max $\Delta T/T$ values of Ag^{2}S NCs (c) and CSS (d) at 1 ps delay for E_{exc} = 3.2 eV. $\Delta T/T$ temporal traces of the Ag$_2$S NCs (e) and CSS (f) at different pump fluences. Data in the marked grey areas reproduce the photobleach resonances and the pale-yellow areas track the excited state absorption evolution.

relaxation, especially at high fluences, what can be tentatively related to the sublinear deviation observed at high fluences in Fig. 3c and d. Considering the significant enhancement of photoluminescence, passivation of surface defects, and stronger saturation of exciton generation, we place further emphasis on CSS.

The temporal evolution of TAS pumped with 3.2 eV photon energy also provides further insights into the order of the decay process. $|\Delta T/T|^{-1}$ evolves linearly with time at longer delays (see section S5, ESI †for more details), indicating that the final recombination is also bimolecular and pointing towards Auger recombination as the dominant relaxation process.[39] It is interesting to note that the $|\Delta T/T|^{-1}$ linear evolution is present in CSS measurements at pump fluences smaller than in Ag$_2$S C, indicating the presence of Auger recombination also at lower fluences on CSS (Fig. S4, ESI†). The effective competition between Auger recombination and defect trapping is another signature of the efficient defect passivation of the CSS NC sample.

Since the model described in eqn (2) and (3) can no longer reproduce our data for CSS NCs pumped at 3.2 eV, we proceed to modify it by introducing two bimolecular processes, as suggested by the observed spectral and temporal evolutions. A well-established approach for experimentally extracting the

dynamics of many-body phenomena is the subtractive procedure.[40] However, its accuracy decreases significantly at high photoexcited state densities, leading to potential artifacts.[41] Considering these limitations, we instead employed global fit analysis as the preferred fitting method using the following photophysical model.

$$\frac{dE_1}{dt} = G - k_1 \times E_1 \tag{4}$$

$$\frac{dE_2}{dt} = k_1 \times E_1 - \gamma_2 \times E_2{}^2 \tag{5}$$

$$\frac{dE_3}{dt} = \gamma_2 \times E_2{}^2 - \gamma_3 \times E_3{}^2 \tag{6}$$

$$\frac{dE_4}{dt} = \gamma_3 \times E_3{}^2 - k_4 \times E_4 \tag{7}$$

where G and k_1 play the same role as in eqn (2) and (3), γ_2 is the rate of biexciton generation, γ_3 is the Auger coefficient and k_4 is the exciton recombination rate. This model satisfactorily reproduces the $\Delta T/T$ dynamics of Ag$_2$S C and CSS over the probed delay window at all the explored pump fluences from 0.16 to 1.29 mJ cm^{-2}.

Fig. 3e displays the temporal dynamics of Ag_2S C at different fluences together with the fits according to eqn (4)–(7), yielding a 500 fs time component as initial thermalization, a biexciton generation coefficient of $\gamma_2 = 1.89 \times 10^{-25}$ s^{-1} m^{-3}, an Auger recombination term of $\gamma_3 = 1.94 \times 10^{-26}$ s^{-1} m^{-3}, and a final exciton recombination with a lifetime of 517 ps. Likewise, a comparison between the temporal traces and fits of CSS NCs is shown in Fig. 3f. In CSS, thermalization of hot excitons occurs in 355 fs lifetime, followed by biexciton formation with a characteristic $\gamma_2 = 9.9 \times 10^{-25}$ s^{-1} m^{-3} and recombination through Auger scattering ($\gamma_3 = 6.7 \times 10^{-26}$ s^{-1} m^{-3}). Finally, the remaining excitons will recombine with a lifetime of 166 ps. It is noteworthy that γ_2 (γ_3) are more than 5 (3) times larger in CSS, implying larger biexciton generation yields and faster non-radiative Auger recombination rates in better passivated NCs. As mentioned before, the PLQY of plain C Ag_2S cores is substantially lower than that of CSS.[20] The observed higher γ_2 and γ_3 rates in CSS compared to those in Ag_2S C are not in conflict with the higher PLQY values in the former measured under photoexcitation conditions where biexciton and Auger recombination are unimportant. However, when pumping with 3.2 eV, differences in surface passivation clearly affect the non-radiative recombination pathways. In particular, the better passivated CSS system exhibits reduced defect-mediated non-radiative recombination, which causes the PLQY increase even if Auger recombination is significant. In contrast, the plain Ag_2S cores suffer from higher defect-mediated recombination, reducing its efficiency (and therefore the PLQY), despite having lower biexciton and Auger constants. A higher biexciton rate constant indicates a faster radiative recombination, which may include both radiative and non-radiative components. Thus, if the radiative component is relevant, it may contribute to the highest PLQY, even if Auger recombination is present.

Hence, the relaxation pathway followed by photoexcited species at low pump fluences starts with an initial sub-picosecond cooling of photoexcited carriers and band to band recombination with a lifetime ranging from hundreds of ps up to a nanosecond, in good agreement with previous work on plain Ag_2S NCs.[17] When the pump fluence increases, two many-body phenomena rule the relaxation dynamics of Ag_2S NCs and CSS: the generation of biexcitons at small delays and Auger recombination as the main band to band relaxation process. Finally the remaining excitons recombine in hundreds of ps.

Conclusions

In summary, we have applied a combination of steady-state absorption, photoluminescence, and femtosecond transient absorption spectroscopy to study the exciton dynamics in Ag_2S-based nanocrystals. The size of these NCs (~8 nm, out of quantum confinement) places them in a regime where bulk-like defects are still important but surface traps are playing an important role in relaxation dynamics. Our results reveal the critical impact of surface passivation on the electronic and optical properties of these nanostructures. While extinction spectra undergo no significant changes upon surface defect passivation, the introduction of passivation layers in the core/shell and core/shell/shell structures leads to a pronounced enhancement of radiative recombination.

Our findings highlight the effectiveness of surface passivation in improving the optical quality of Ag_2S-based nanocrystals and underscore the importance of controlling the exciton density for studying many-body interactions in these materials. We have found that the core/shell/shell system shows reduced trap-mediated paths and faster multi-exciton recombination dynamics. These NCs, in particular, demonstrate significant promise for optoelectronic and nanomedicine applications, where enhanced photoluminescence and reduced nonradiative recombination are desirable.

Author contributions

P.W., R.M.M and E.M.R.: preparation of NCs and data interpretation. S.G.O. and J.C.-G.: spectroscopic measurements and data interpretation. V.V.-M.: spectroscopic measurements, data analysis, writing the original draft, reviewing, conceptualization, and methodology. B.H.J.: writing the original draft, reviewing, conceptualization, methodology, and editing. All authors revised and contributed to the final version of the manuscript.

Data availability

The data supporting this article have been included in the ESI.† It can be found in the webpage **https://www.victorvega-mayo.com** or upon request to the corresponding authors. All research data related to this article will be published in the DIGITAL.CSIC repository at **https://digital.csic.es/?locale=en** and in the IMDEA Nanoscience public repository.

Conflicts of interest

All authors declare no conflicts of interest.

Acknowledgements

References

1 E. Desurvire, *Erbium-Doped Fiber Amplifiers: Principles and*, Wiley-VCH Verlag GmbH & Co., 2002.

2 Y. Liu, J. Li, J. Xiagou and Z. Liu, Recent Advances in NIR or X-ray Excited Persistent Luminescent Materials for Deep Bioimaging, *J. Fluoresc.*, 2025, **35**, 179–195.

3 J. Feng, X. Li, Z. Shi, C. Zheng, X. Li, D. Leng, Y. Wang, J. Liu and L. Zhu, 2D Ductile Transition Metal Chalcogenides (TMCs): Novel High-Performance Ag_2S Nanosheets for Ultrafast Photonics, *Adv. Opt. Mater.*, 2019, **8**(6), 1901762.

4 D. Franke, D. K. Harris, O. Chen, O. T. Bruns, J. A. Carr, M. W. B. Wilson and M. G. Bawendi, Continuous injection synthesis of indium arsenide quantum dots emissive in the short-wavelength infrared, *Nat. Commun.*, 2016, **7**, 12749.

5 A. M. Smith, M. C. Mancini and S. Nie, Second window for in vivo imaging, *Nat. Nanotechnol.*, 2009, **4**, 710–711.

6 S. Kasap, P. Capper and C. Koughia, *Springer handbook of electronic and photonic materials*, Springer US, 2007.

7 A. J. Nozik, Quantum dot solar cells, *Physica E Low Dimens. Syst. Nanostruct.*, 2002, **14**, 115–120.

8 J. Zhou, B. del Rosal, D. Jaque, S. Uchiyama and D. Jin, Advances and challenges for fluorescence nanothermometry, *Nat. Methods*, 2020, **17**, 967–980.

9 Y. Shen, J. Lifante, E. Ximendes, H. D. A. Santos, D. Ruiz, B. H. Juarez, I. Z. Gutierrez, V. T. Vera, J. R. Retama, E. M. Rodriguez, D. H. Ortgies, D. Jaque, A. Benayas and B. del Rosal, Perspectives for Ag_2S NIR-II nanoparticles in biomedicine: from imaging to multifunctionality, *Nanoscale*, 2019, **11**, 19251–19264.

10 A. Tubtimtae, K. L. Wu, H. Y. Tung, M. W. Lee and G. J. Wang, Ag_2S quantum dot-sensitized solar cells, *Electrochem. Commun.*, 2010, **12**, 1158–1160.

11 D. G. Moon, S. Rehan, D. H. Yeon, S. M. Lee, S. Ahn and Y. Cho, A review on binary metal sulfide heterojunction solar cells, *Sol. Energy Mater. Sol. Cells*, 2019, **200**, 109963.

12 R. J. Ellingson, M. C. Beard, J. C. Johnson, P. Yu, O. I. Micic, A. J. Nozik, A. Shabaev and A. L. Efros, Highly Efficient Multiple Exciton Generation in Colloidal PbSe and PbS Quantum dots, *Nano Lett.*, 2005, **5**, 865–871.

13 R. D. Schaller and V. I. Klimov, High efficiency Carrier Multiplication in PbSe Nanocrystals: implications for Solar energy Conversions, *Phys. Rev. Lett.*, 2004, **92**, 186601.

14 J. Sun, W. Yu, A. Usman, T. T. Isimjan, S. Dgobbo, E. Alarousu, K. Takanabe and O. F. Mohammed, Generation of Multiple Excitons in Ag_2S Quantum Dots: Single High-Energy versus Multiple-Photon Excitation, *J. Phys. Chem. Lett.*, 2014, **5**, 659–665.

15 S. Kolodinski, J. H. Werner, T. Wittchen and H. J. Queisser, Quantum efficiencies exceeding unity due to impact ionization in silicon solar cells, *Appl. Phys. Lett.*, 1993, **63**, 2405–2407.

16 S. Lin, Y. Feng, X. Wen, P. Zhang, S. Woo, S. Shrestha, G. Conibeer and S. Huang, Theoretical and Experimental Investigation of the Electronic Structure and Quantum Confinement of Wet-Chemistry Synthesized Ag_2S Nanocrystals, *J. Phys. Chem. C*, 2015, **119**, 867–872.

17 M. C. Brelle, J. Z. Zhang, L. Nguyen and R. Mehra, Synthesis and Ultrafast Study of Cysteine- and Glutathione-Capped Ag_2S Semiconductor Colloidal Nanoparticles, *J. Phys. Chem. A*, 1999, **103**, 10194–10201.

18 M. S. Smirnov, O. V. Ovchinnikov, A. I. Zvyagin, S. A. Tikhomirov, A. N. Ponyavina, V. A. Povedailo, N. T. Binh and P. H. Minh, Transient Absorption Dynamics and Nonlinear Optical Response in Colloidal Ag_2S Quantum Dots, *Opt. Spectrosc.*, 2022, **130**, 224–231.

19 P. Peng, B. Sadtler, A. P. Alivisatos and R. J. Saykally, Exciton Dynamics in CdS–Ag_2S Nanorods with Tunable Composition Probed by Ultrafast Transient Absorption Spectroscopy, *J. Phys. Chem. C*, 2010, **114**, 5879–5885.

20 P. Wang, R. Morales-Márquez, G. Cervás, A. Hernandez Medel, M. Paris Ogayar, D. Jimenez de Aberasturi, A. I. Isidro-Gomez, A. Torres-Pardo, F. J. Palomares, S. Garcia-Örrit, C. T. Sousa, A. Espinosa, H. H. Telle, D. H. Ortgies, V. Vega-Mayoral, J. Cabanillas-Gonzalez, E. Martin Rodriguez, U. Resch-Genger, K. D. Wegner and B. H. Juarez, The role of temperature in the photoluminescence quantum yield (PLQY) of Ag_2S-based nanocrystals, *Mater. Horiz.*, 2024, **11**, 6158–6168.

21 Y. Zhang, Y. Liu, C. Li, X. Chen and Q. Wang, Controlled Synthesis of Ag_2S Quantum Dots and Experimental Determination of the Exciton Bohr Radius, *J. Phys. Chem. C*, 2014, **118**, 4918–4923.

22 Y.-M. Zeng, L. J. Pan, J. Wang, Y.-L. Fan, Y. Shu, D.-W. Pang and Z.-L. Zhang, Interfacial Synthesis of Ag_2S/ZnS Core/Shell Quantum Dots in a Droplet Microreactor, *ChemistrySelect*, 2020, **5**, 5889–5894.

23 M. C. Beard, K. P. Knutsen, P. Yu, J. M. Luther, Q. Song, W. K. Metzger, R. J. Ellingston and A. J. Nozik, Multiple Exciton Generation in Colloidal Silicon Nanocrystals, *Nano Lett.*, 2007, **7**, 2506–2512.

24 W. J. Mir, Q. Swarnkar, R. Sharma, A. Katti, K. V. Adarsh and A. Nag, Origin of Unusual Excitonic Absorption and Emission from Colloidal Ag_2S Nanocrystals: Ultrafast Photophysics and Solar Cell, *J. Phys. Chem. Lett.*, 2015, **6**, 3915–3922.

25 J. W. de Wit, I. Zabala-Gutierrez, R. Marin, A. Zhakeyev, S. Melle, O. G. Calderon, J. Marques-Hueso, D. Jaque, J. Rubio-Retama and A. Meijerink, New Insights in Luminescence and Quenching Mechanisms of Ag_2S, *J. Phys. Chem. Lett.*, 2024, **15**, 8420–8426.

26 I. Zabala gutierrez, C. Gerke, Y. Shen, E. Ximendes, M. Manso Silvan, R. Marin, D. Jaque, O. G. Carderón, S. Melle and J. Rubio-Retama, Boosting the Near-Infrared Emission of Ag_2S Nanoparticles by a Controllable Surface Treatment for Bioimaging Applications, *ACS Appl. Mater. Interfaces*, 2022, **14**, 4871–4881.

27 S. Sadovnikov and A. I. Gusev, Recent progress in nano-structured silver sulfide: from synthesis and nonstoichiometry to properties, *J. Mater. Chem. A*, 2017, **5**, 17676–17704.

28 J. Cabanillas-Gonzalez, G. Grancini and G. Lanzani, Pump-Probe Spectroscopy in Organic Semiconductors: Monitoring Fundamental Processes of Relevance in Optoelectronics, *Adv. Mater.*, 2011, **23**, 5468–5485.

29 V. Vega-Mayoral, D. Vella, T. Borzda, M. Prijatelj, I. Tempra, E. Pogna, S. Dal Conte, P. Topolovsek, N. Vujicic, G. Cerullo, D. Mihailovic and C. Gadermaier, Exciton and charge carrier dynamics in few-layer WS_2, *Nanoscale*, 2016, **8**, 5428–5434.

30 V. I. Klimov, S. A. Ivanov, J. Nanda, M. Acherman, I. Bezel, J. A. McGuire and A. Piryatinski, Single-exciton optical gain in semiconductor nanocrystals, *Nature*, 2007, **447**, 441–446.

31 J. Cabanillas-Gonzalez, T. Virgili, A. Gambetta, G. Lanzani, T. Anthopoulos and D. M. Leeuw, Photoinduced Transient Stark Spectroscopy in Organic Semiconductors: A Method for Charge Mobility Determination in the Picosecond Regime, *Phys. Rev. Lett.*, 2006, **96**, 106601.

32 C. Gadermaier, E. Menna, M. Meneghetti, W. J. Kennedy, Z. V. Vardeny and G. Lanzani, Long-lived charged states in single-walled carbon nanotubes, *Nano Lett.*, 2006, **6**, 301–305.

33 Q. C Sun, L. Yadgarov, R. Rosentsveig, G. Seifert, R. Tenne and J. L. Musfeldt, Observation of a Burstein-Moss shift in rhenium-doped MoS_2 nanoparticles, *ACS Nano*, 2013, **7**, 3506–3511.

34 E. Pogna, M. Marsili, D. De Fazio, S. Dal Conte, C. Manzoni, D. Sangali, D. Yoon, A. Lombardo, A. C. Ferrari, A. Marini, G. Cerullo and D. Prezzi, Photo-Induced Bandgap Renormalization Governs the Ultrafast Response of Single-Layer MoS_2, *ACS Nano*, 2016, **10**, 1182–1188.

35 F. Aparicio, I. Sancho-Casado, P. Chamorro, M. Gonzalez-Sanchez, S. Pujals, V. Vega-Mayoral and D. Gonzalez-Rodriguez, Self–Assembly of Chemically Programmed Amphiphiles into Aqueous Nanotubes with a Lipophilic Lumen, *Chem. – Eur. J.*, 2024, **30**, e202402365.

36 V. Vega-Mayoral, T. Borzda, D. Vella, M. Prijatelj, E. Pogna, C. Backes, J. Coleman, G. Cerullo, D. Mihailovic and C. Gadermaier, Charge trapping and coalescence dynamics in few layer MoS_2, *2D Mater.*, 2018, **5**, 015011.

37 E. J. Sie, A. J. Frenzel, Y. H. Lee, J. Kong and N. Gedik, Intervalley biexcitons and many-body effects in monolayer MoS_2, *Phys. Rev. B*, 2015, **92**, 125417.

38 A. Chernikov, C. Ruppert, H. M. Hill, A. F. Rigosiu and T. F. Heinz, Population inversion and giant bandgap renormalization in atomically thin WS_2 layers, *Nat. Photonics*, 2015, **9**, 466–470.

39 L. Yuan, T. Wang, T. Zhu, M. Zhou and L. Huang, Excityon dynamics, transport and annihilation in atomically thin two-dimensional semiconductors, *J. Phys. Chem. Lett.*, 2017, **8**, 3371–3379.

40 V. I. Klimov, A. A. Mikhailovsky, D. W. McBranch, C. A. Leatherdale and M. G. Bawendi, Quantization of Multiparticle Auger Rates in Semiconductor Quantum Dots, *Science*, 2000, **287**, 1011–1013.

41 V. I. Klimov, J. A. McGuire, R. D. Schaller and V. I. Rupasov, Scaling of multiexciton lifetimes in semiconductor nanocrystals, *Phys. Rev. B*, 2008, **77**, 195324.